Determining Pore Sizes Using an Internal Magnetic Field

Yi-Qiao Song

Schlumberger-Doll Research, Old Quarry Road, Ridgefield, Connecticut 06877

A concept is proposed to measure the pore size length scale by the internal magnetic field (B_i) in porous materials. The spatial distribution of the magnetic field inhomogeneity, a result of the magnetic susceptibility contrast between the porous material and the fluid, reflects the underlying pore geometry. Diffusion in B_i causes the initial decay of magnetization. At long times, the effect of B_i saturates when the diffusion length reaches a characteristic pore size. This method is independent of surface spin relaxation in determining pore sizes. Nuclear magnetic resonance experiments on packed glass beads and sedimentary rock samples will be presented.   © 2000 Academic Press

Key Words: internal magnetic field; diffusion; stimulated echo; pore size.

INTRODUCTION AND THEORY

Although porous materials abound in our environment ranging from naturally occurring rocks and woods to man-made materials such as concrete and food products, the characterization of the internal geometry of such materials is by no means simple. Statistical description of the pore space, such as the average pore size, is often most useful in understanding the physical properties of the materials, such as permeability to fluid flow. Among many experimental methods, such as gas BET and mercury capillary pressure, nuclear magnetic resonance has been used successfully to measure the surface-to-volume ratio ($\langle S/V \rangle$) via spin relaxation (*1*) and to study pore structure using pulsed field gradient (PFG) techniques (*2, 3*). From $\langle S/V \rangle$, one may deduce a pore size: $d \equiv 6/\langle S/V \rangle$. However, in materials with surface roughness and complex surface relaxivity such as is due to microporosity, inclusion of clay, and deviation from the fast diffusion condition, the interpretation of the spin relaxation behavior might not be straightforward to determine $\langle S/V \rangle$ or the pore size distribution.

When a porous material is subject to a uniform external magnetic field (B_0), an inhomogeneous magnetic field (B_i) appears inside the pore space, due to the difference of the magnetic susceptibility (χ) between the solid materials and the pore-filling fluid. One may estimate the magnitude of the internal field to be $\sim \Delta \chi B_0$, where $\Delta \chi$ is the difference in susceptibilities. The gradients of the internal field can be rather

large in sedimentary rocks and other materials (*4–6*) and can cause problems in magnetic resonance imaging (*7*) and measurements of the diffusion constant and spin relaxation (*2, 8, 9*).

We take the point of view that the internal magnetic field is a representation of the underlying geometry and describe here a method to explore the *statistical* properties of B_i in order to characterize pore geometry. We propose an experiment to characterize the nuclear spin magnetization decay due to diffusion in the internal field (DDif) and obtain the pore length scale in terms of the diffusion behavior. We have used this method to study the water diffusion behavior in packed bead samples of varying sizes and a sedimentary rock sample.

The simplest form of the proposed experiment involves application of a series of three radiofrequency (RF) pulses at the Larmor frequency of the nuclear spin, separated by time intervals t_e and t_d:

$$\frac{\pi}{2}-t_e-\frac{\pi}{2}-t_d-\frac{\pi}{2}-t_e-\text{echo}. \qquad [1]$$

We denote the echo signal by $E(t_d)$. The notation $\pi/2$ denotes a RF pulse that rotates the spin vector by 90°. The sequence, called the stimulated echo sequence, was introduced by Hahn (*8*) and has been widely used in combination with applied magnetic field gradients to measure diffusion constants (*10*) and to study the structure of porous materials (*3, 11*). In our experiments, no applied gradients are necessary. In order to calibrate the effect of the spin–lattice (T_1) relaxation, the following sequence is used: $\frac{\pi}{2}-t_e-\pi-t_e-\frac{\pi}{2}-t_d-\frac{\pi}{2}$–FID, and the free-induction decay (FID) signal is acquired as the reference, $R(t_e, t_d)$. The π pulse cancels the phase accumulation due to B_i and the FID signal measures only the effect of spin–lattice relaxation during t_d. Effects of the spin–spin relaxation during t_e are partially compensated by this sequence.

Neglecting relaxation, the echo intensity can be shown to follow the equation below:

$$E(t_e, t_d) = \int d\mathbf{x}_1 d\mathbf{x}_2 e^{i\gamma t_e[B_i(\mathbf{x}_1)-B_i(\mathbf{x}_2)]} P(\mathbf{x}_1, \mathbf{x}_2, t_d), \qquad [2]$$

where $B_i(\mathbf{x})$ is the internal magnetic field and γ is the gyro-

magnetic ratio of the probed spins. $\mathbf{x}_1$ and $\mathbf{x}_2$ are the initial and the final positions of a spin and $P(\mathbf{x}_1, \mathbf{x}_2, t_d)$ is the magnetization diffusion propagator, the probability of the spin magnetization to diffuse from $\mathbf{x}_1$ to $\mathbf{x}_2$ during time t_d. For $t_e \ll t_d$, we will neglect diffusion during t_e and focus on the diffusion effect during t_d. At large t_d, the diffusion distance may be as large as the pore size, thus we will consider the full spatial dependence of $B_i(\mathbf{x})$.

At short t_d, the diffusion causes an incomplete refocusing since $\langle[B_i(\mathbf{x}_1) - B_i(\mathbf{x}_2)]^2\rangle \neq 0$, thus the echo decays, similar to the case of applied field gradients (8). Unlike the applied gradients, a crucial character is that B_i *is bounded in magnitude and the field variation occurs over the pore length scale.* This leads to a long-time asymptote of the signal independent of t_d, and the time scale to reach this limit is the diffusion time across the pore dimension.

One may rewrite Eq. [2] in terms of the magnetic field,

$$E(t_e, t_d) = \int_{B_{min}}^{B_{max}} dB_1 dB_2 \times e^{i\gamma t_e[B_1 - B_2]}\tilde{P}(B_1, B_2, t_d), \quad [3]$$

where $\tilde{P}(B_1, B_2, t)$ is the diffusion propagator in the B_i space. The general form of $\tilde{P}(B_1, B_2, t)$ may be difficult to evaluate; however, we may draw an analogy from the spatially bound diffusion. For diffusion in a box of dimension d, the mean square displacement will rise at early time and saturates at d^2 when the diffusion length is comparable to d, i.e., $t \sim d^2/2D_0$. D_0 is the bulk diffusion constant.

Similarly for the diffusion in the bound B space, $\tilde{P}(B_1, B_2, t)$ will approach $f(B_1)f(B_2)$ ($f(B)$ is the magnetic field distribution function), uncorrelated with respect to B_1 and B_2, when the molecule has explored the entire B_i space at large t_d. In this limit, Eq. [3] can be evaluated,

$$E(t_e, t_d \to \infty) = \left| \int dB e^{i\gamma t_e B} f(B) \right|^2, \quad [4]$$

independent of t_d. Furthermore, it is the square of the magnitude of the free-induction-decay signal at time t_e.

RESULTS AND DISCUSSION

Measurements were made to determine $E(t_d)$ and $R(t_d)$ for several randomly packed bead samples of 30, 50, and 100 μm average diameter. NMR experiments were performed at a magnetic field of 2.14 T and the $\pi/2$ pulse length is 3 μs. t_e is usually 1 ms or shorter and the list of t_d is usually 25 or more data points between 1 ms and several seconds. For the 30-μm sample, the t_e used was shorter.

The original data of $E(t_d)$ and $R(t_d)$ for the 50-μm bead sample are shown in Fig. 1A. The reference signal shows a single-exponential decay for over two orders of magnitude and
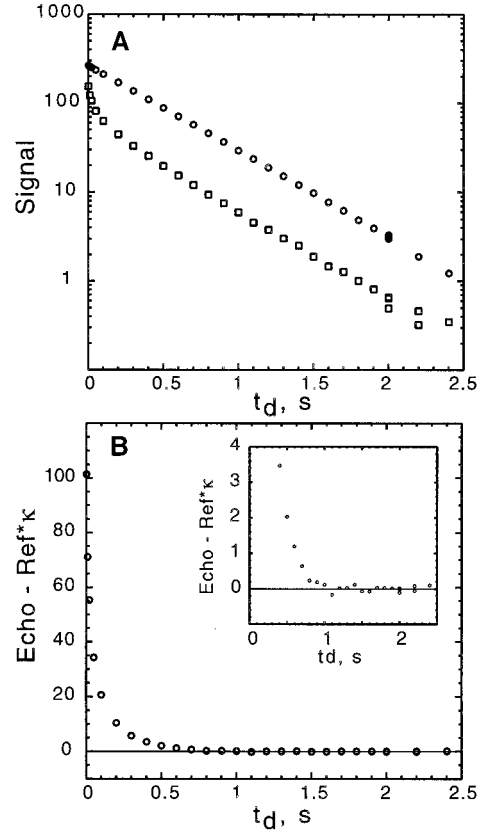
FIG. 1. (A) The echo ($\square$) and the reference ($\bigcirc$) signals as a function of t_d. (B) The additional decay appeared in the echo signal due to an internal field, obtained by $E(t_d) - R(t_d)\kappa$. κ is determined by the ratio E/R at large t_d. The inset in (B) shows the details of $E(t_d) - R(t_d)\kappa$ approaching zero. The sample was made of randomly packed glass beads (Duke Scientific Corp.) of 50-μm average diameter. The samples were saturated with water in 5-mm NMR tubes. NMR measurements were performed using a homebuilt probe on a Tecmag spectrometer at a magnetic field of 2.14 T (Nalorac Cryogenics, Inc.).

thus the relaxation is in the fast diffusion limit due to weak surface relaxation. However, the echo signal shows a dramatic fast decay at the short t_d. This additional decay in $E(t_d)$ is due to diffusion in the internal field. When t_d increases, the decay rate of E approaches that of the reference signal and for $t_d > 1$ s the two data sets are parallel in the semilog plot (Fig. 1A). In order to separate the effect of the internal field, we calculate $E(t_d) - R(t_d)\kappa$, shown in Fig. 1B and its inset. The parameter κ is determined by the ratio E/R for $t_d > 1$ s. The critical time constant $t_{DDif} = 1$ s can be defined as the time when the B_i-induced decay approaches zero.

Figure 2 shows the data for the 100- (A) and 30-μm beads (B). Similar to the data for the 50-μm bead sample, the internal field effect decreases as t_d increases and the t_{DDif} can be obtained as 3.5 and 0.5 s for the two samples, respectively.

In order to obtain the diffusion length scale at t_{DDif}, we have calculated the mean square displacement ($\langle r(t_d)^2 \rangle$) of water molecules as a function of diffusion time t_d. In porous materials, the effective diffusion constant of water is reduced com-
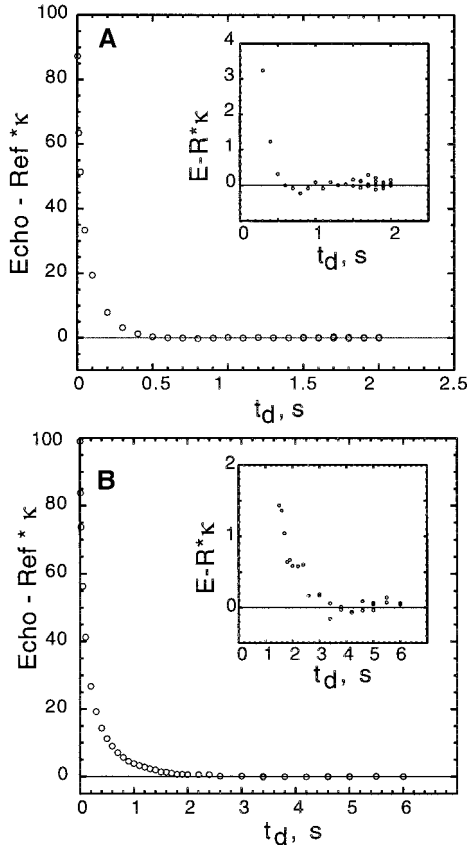
FIG. 2. The internal field induced decay, $E(t_d) - R(t_d)\kappa$, for samples of (A) 100-μm beads and (B) 30-μm beads. The insets show the regions where $E(t_d) - R(t_d)\kappa$ approaches zero. κ is determined by the ratio E/R at large t_d for each sample.

pared to the bulk diffusion constant D_0 due to restriction (12). This behavior has been characterized in terms of a time-dependent diffusion constant $D(t_d)$ (13, 14) and an approximation was given in Ref. (15):

$$\frac{D(t)}{D_0} = 1 - \left(1 - \frac{1}{\alpha}\right)$$

$$\times \frac{c\sqrt{t} + (1 - 1/\alpha)t/\theta}{(1 - 1/\alpha) + c\sqrt{t} + (1 - 1/\alpha)t/\theta}, \quad [5]$$

where $c = (4/9\sqrt{\pi})(S/V)\sqrt{D_0}$. For packed beads of diameter d, $\sqrt{D_0\theta}/d \approx 0.15$, $\alpha = 1/0.64$, and the surface-to-volume ratio $S/V = 9.8/d$. Using the above equation, the mean displacement can be calculated as $\Delta r(t) \equiv \sqrt{2D(t)t}$ for individual bead size. The diffusion length scale defined by $\Delta r(t_{DDif})$ is listed in Table 1 and it corresponds well to the bead diameters of the corresponding samples. This result demonstrates the utility of Δr (or t_{DDif}) as a measure of the pore dimension.

According to Eq. [4], the reduction of the echo signal, normalized by the effect of T_1 relaxation, is independent of t_d

TABLE 1
Bead Sizes and the Measured Δr_{DDif} and l_{DDif}

Sample	Bead diameter (μm)	Δr_{DDif} (μm)	$l_{DDif} \equiv \sqrt{2D_0 t_{DDif}}$ (μm)
A	30.6	34 ± 3	42 ± 4
B	50	52 ± 5	59 ± 5
C	105	100 ± 10	110 ± 10
Fontainebleu 2	—	—	52

Note. The water diffusion constant (D_0) is taken to be 1.77×10^{-5} cm^2/s.

at long t_d. This is shown in Fig. 3 for the 30-μm bead sample. The T_1-normalized E was found a constant for $t_d > 0.4$ s and the data at $t_d = 0.4$ and 1 s were plotted in Fig. 3. The t_e dependence of the normalized E is consistent with the square of the FID signal shown as the line, in good agreement with Eq. [4].

We have also performed experiments on a sedimentary rock sample, Fontainebleau 2, used in a previous study (16). The measured echo height showed a behavior very similar to the observation from the packed bead sample, namely the initially decay and the eventual constant echo height. A critical time can be obtained, $t_{DDif} = 0.75 \pm 0.05$ s, and a critical length can be defined: $l_{DDif} \equiv \sqrt{2D_0 t_{DDif}} = 52$ μm, where $D_0 = 1.77 \times 10^{-5}$ cm^2/s is the bulk water diffusion constant at room temperature. Although a close approximation between the bead diameter and $\Delta r(t)$ was observed for the packed bead samples, we do not expect it to be exact for general geometry. The shape of the pores as well as the grain size distribution will undoubtedly alter the magnetic field distribution as characterized by $E(t_e, t_d)$. Previous measurements of the time-dependent diffusion constants (16) determined $1/\langle S/V \rangle = 7.1$ μm and thus
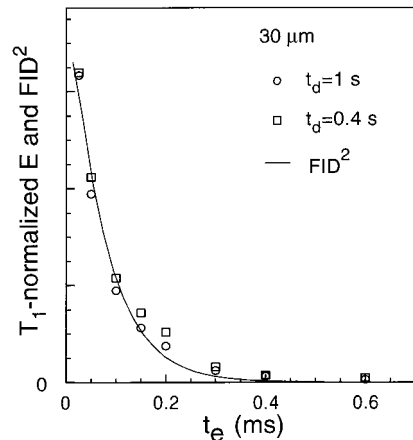
FIG. 3. The T_1-normalized E as a function of t_e at long t_d for the sample made of 30-μm-diameter beads. The T_1-normalized E becomes a constant around $t_d = 0.4$ s and the data are shown for $t_d = 0.4$ and 1 s. The line is the square of the FID signal acquired by a $\pi/2$ pulse. According to Eq. [4], $E(t_e, t_d \to \infty) = |FID(t_e)|^2$, consistent with the measurement.
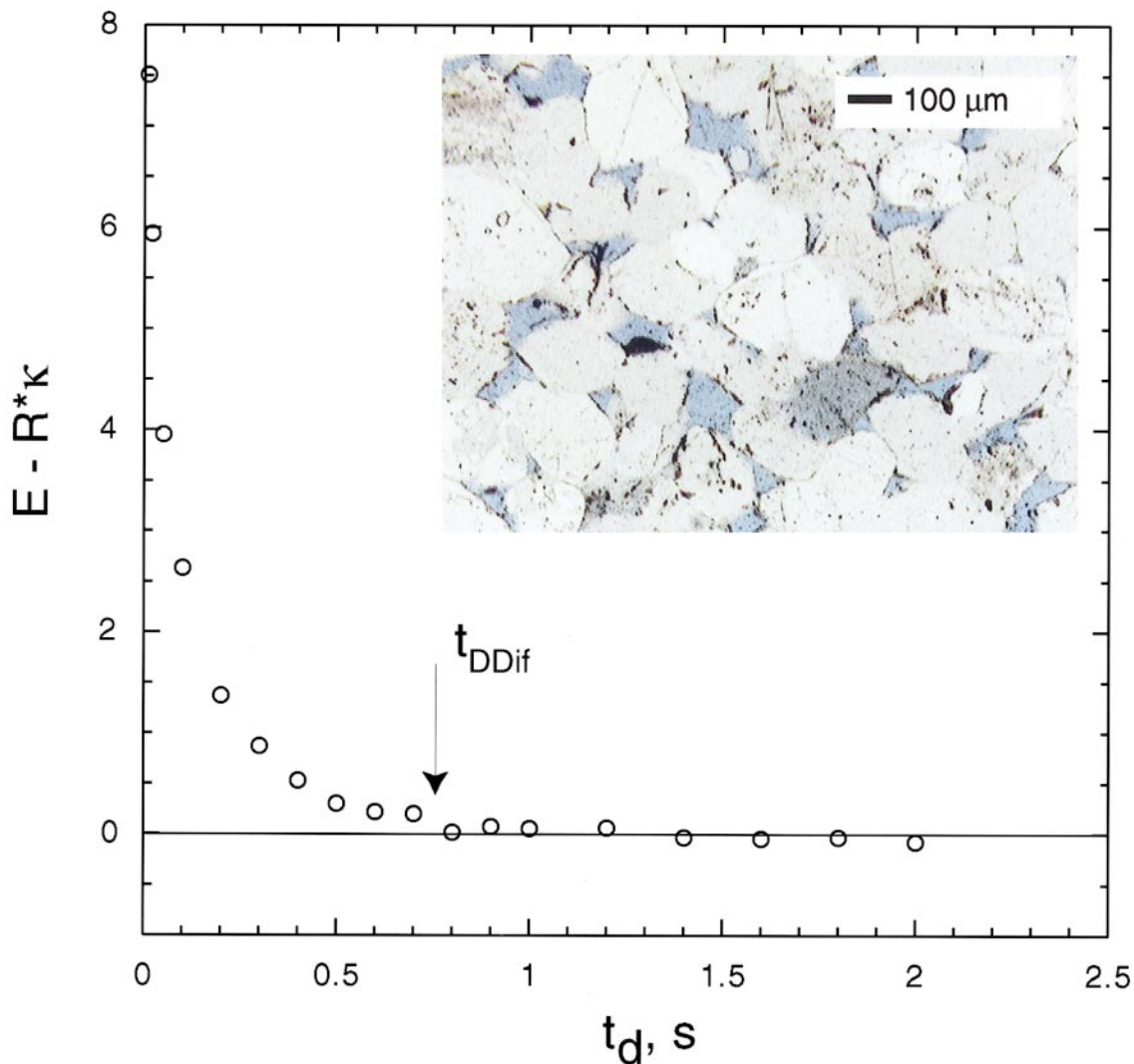
FIG. 4. DDif measured for a sandstone rock sample (Fontainebleau 2). The internal field induced decay is shown by $E(t_d) - R(t_d)\kappa$, a critical time constant t_{DDif} is obtained to be 0.75 s, and $l_{DDif} = 52$ μm. The inset shows an image of the thin section of the sample. The blue regions are the pore space filled with the blue epoxy before the sample was prepared. The size of the large pores is approximately 100 μm.

one may estimate the pore diameter to be $6/\langle S/V \rangle \approx 42$ μm for spherical pores. A cross-sectional image of the sample (inset of Fig. 4) is obtained by optical transmission microscopy from a 30-μm section of the sample. The pore space is represented by the blue regions because of the blue epoxy impregnation prior to sectioning, showing the size of the large pore to be 100 μm.

CONCLUSIONS

The susceptibility contrast ($\Delta\chi$) of water and sedimentary rocks varies from 10^{-6} to 10^{-4} (SI unit) and an internal magnetic gradient as high as 10 T/m may be present at 50 mT (6). The magnitude of the internal field induced decay is determined by $\gamma t_e \Delta\chi B_0$, an experimentally controlled quantity. This leads to one of the advantages of this method that the

signal loss due to diffusion can be very low. For example, a 10–20% decay in E is adequate in contrast to the rather significant decay of signal in a conventional PFG experiment (3).

This experiment can be performed at a variety of magnetic fields, especially at high magnetic fields where t_e can be shortened to extend the minimum detectable length scale to submicrometers. The maximum detectable length using water is approximately 100 μm, limited by the relaxation time. In addition, this technique can be used with any NMR-sensitive nuclei, such as xenon gas, to enhance the maximum detectable length scale to millimeters.

In summary, we have demonstrated the validity of a new method for characterizing pore sizes in packed-bead samples and sandstone rock. The concept is based on the variation of

the internal magnetic field and is independent of the surface relaxation properties. The experimental implementation is simple and without the use of pulsed field gradients. This technique may be applied to the study of the complex geometry of materials such as sedimentary rock, cement, membranes, and biological media.

REFERENCES

1. For recent reviews, see W. P. Halperin, F. D'Orazio, S. Bhattacharja, and J. C. Tarczon, *in* "Molecular Dynamics in Restricted Geometries" (J. Klafter and J. M. Drake, Eds.), Chap. 3, Wiley, New York (1989); W. E. Kenyon, *Nucl. Geophys.* **6**, 153 (1992).

2. E. O. Stejskal and J. E. Tanner, *J. Chem. Phys.* **42**, 288 (1965).

3. P. T. Callaghan, A. Coy, D. MacGowan, K. J. Packer, and F. O. Zelaya, *Nature* **351**, 467 (1991).

4. R. M. Weisskoff, C. S. Zuo, J. L. Boxerman, and B. R. Rosen, *Magn. Reson. Med.* **31**, 601 (1994); G. C. Borgia, R. J. S. Brown, and P. Fantazzini, *Magn. Reson. Imaging* **14**, 731 (1996).

5. M. D. Hurlimann, K. G. Helmer, and C. H. Sotak, *Magn. Reson. Imag.* **16**, 535 (1997).

6. M. D. Hurlimann, *J. Magn. Reson.* **131**, 232–240 (1998).

7. P. T. Callaghan, "Principles of Nuclear Magnetic Resonance Microscopy," Oxford Univ. Press, New York (1993).

8. E. L. Hahn, *Phys. Rev.* **80**, 580 (1950).

9. R. M. Cotts, M. J. R. Hoch, T. Sun, and J. T. Markert, *J. Magn. Reson.* **83**, 252 (1989).

10. J. E. Tanner, *J. Chem. Phys.* **52**, 2523 (1970).

11. R. M. Cotts, *Nature* **351**, 443 (1991).

12. D. E. Woerssner, *J. Phys. Chem.* **67**, 1365 (1963).

13. R. C. Wayne and R. M. Cotts, *Phys. Rev.* **151**, 264 (1966).

14. P. P. Mitra, P. N. Sen, L. M. Schwartz, and P. Le Doussal, *Phys. Rev. Lett.* **68**, 3555 (1992).

15. L. L. Latour, P. P. Mitra, R. L. Kleinberg, and C. H. Sotak, *J. Magn. Reson. A* **101**, 342–346 (1993).

16. M. D. Hurlimann, K. G. Helmer, L. L. Latour, and C. H. Sotak, *J. Magn. Reson. A* **111**, 169–178 (1994).